SCIENCE CHINA Materials ARTICLES

mater.scichina.com link.springer.com

Published online 22 January 2017 | doi: 10.1007/s40843-016-5166-0
Sci China Mater 2017, 60(4): 315–323

Synthesis and electrochemical performance of Sn-doped $LiNi_{0.5}Mn_{1.5}O_4$ cathode material for high-voltage lithium-ion batteries

Jingmin Hao[1], Haiping Liu[1*], Yuanpeng Ji[1] and Sifu Bi[2]

ABSTRACT **$LiNi_{0.5}Mn_{1.5-x}Sn_xO_4$ ($0 \le x \le 0.1$) cathode materials with uniform and fine particle sizes were successfully synthesized by a two-step calcination of solid-state reaction method. As the cathode materials for lithium ion batteries, the $LiNi_{0.5}Mn_{1.48}Sn_{0.02}O_4$ shows the highest specific capacity and cycle stability. In the potential range of 3.5–4.9 V at room temperature, $LiNi_{0.5}Mn_{1.48}Sn_{0.02}O_4$ composite material shows a discharge capacity of more than 117 mA h g^{-1} at 0.1 C, while the corresponding discharge capacity of undoped $LiNi_{0.5}Mn_{1.5}O_4$ is only 101 mA h g^{-1}. Moreover, in cycle performance, all the $LiNi_{0.5}Mn_{1.5-x}Sn_xO_4$ ($0 \le x \le 0.1$) samples show better capacity retention than the undoped $LiNi_{0.5}Mn_{1.5}O_4$ at 1 C rate after 100 cycles. Especially, for the $LiNi_{0.5}Mn_{1.5}O_4$, the discharge capacity after 100 cycles is 90 mA h g^{-1}, while the corresponding discharge capacities of the undoped $LiNi_{0.5}Mn_{1.5}O_4$ is only 56.1 mA h g^{-1}. The significantly enhanced D_{Li^+} and the enlarged electronic conductivity make the Sn-doped spinel $LiNi_{0.5}Mn_{1.5}O_4$ material present even more excellent electrochemical performances. These results reveal that Sn-doping is an effective way to improve electrochemical performances of $LiNi_{0.5}Mn_{1.5}O_4$.**

Keywords: cathode material, Sn doping, lithium-ion battery, two-step calcination

INTRODUCTION

Recently, the Li-ion battery has been considered a potential energy source for the electric vehicle and hybrid electric vehicle because of its high energy density and long cycle life [1]. Among numerous transition metal oxides applied to the cathode in Li-ion batteries, the Ni-doped manganese spinel oxide $LiNi_{0.5}Mn_{1.5}O_4$ has become one of the most promising and attractive candidates due to its excellent properties such as high voltage (4.8 V *vs.* Li/Li^+) [2], three-dimensional lithium ion diffusion paths in the spinel lattice, low cost of raw materials, and environmental friendliness.

However, spinel $LiNi_{0.5}Mn_{1.5}O_4$ suffers from a corrosion reaction between the cathode surface and the electrolyte at 5 V, leading to poor rate stability, especially at elevated temperatures [3–4]. Hence, $LiNi_{0.5}Mn_{1.5}O_4$ still has non-negligible capacity fading during cycling due to the structural and chemical instabilities resulting from the presence of Mn^{3+} ions. To solve this problem, researchers have put forth many solutions such as surface-coating [5–7], nanostructuring [2], and cationic-doping with ions such as Mo^{6+} [8], Cr^{3+} [9], B^{3+} [10], Ti^{4+} [11], Al^{3+} [12], and W^{4+} [13]. All these doped metal cations can induce differences in the cycle properties and electrical conductivity of $LiNi_{0.5}Mn_{1.5}O_4$ to different extents. In most cases, a stable structure, minimized polarization, and improved electrical conductivity were obtained via substitution. However, some doping metals could also have detrimental effects. To the best of our knowledge, Sn doping has been reported to be favorable in $Li_3V_{2-x}Sn_x(PO_4)_3/C$ [14], $LiNi_{0.8-x}Co_{0.2}Sn_xO_2$ [15], $Li_{3.9}Sn_{0.1}Ti_5O_{12}$ [16], $LiFe_{1-x}Sn_xPO_4/C$ [17], and other Li-based materials. Nevertheless, little attention has been paid to Sn-doping in $LiNi_{0.5}Mn_{1.5}O_4$ materials.

$LiNi_{0.5}Mn_{1.5}O_4$ has been synthesized by various methods including solid-state reactions [3,18–20], sol–gel synthesis [9,21], co-precipitation [22,23], spray pyrolysis [24], electrophoretic deposition [25], pulsed laser deposition [26], molten salt method [27], emulsion drying [28], and hydrothermal method [29]. Among these methods, the wet chemical method shows high phase purity and excellent electrochemical performance in general, but at the cost of complicated technique and high production

[1] School of Marine Science and Technology, Harbin Institute of Technology, Weihai 264209, China
[2] School of Materials Science and Engineering, Harbin Institute of Technology, Weihai 264209, China
[*] Corresponding author (email: hpliuhit@126.com)

cost, which makes the wet chemical method difficult to apply in practice. In contrast, the solid-state method is facile, cheap, and easy to industrialize. Wang *et al.* [3] synthesized $LiNi_{0.5}Mn_{1.5}O_4$ through a two-step calcination method with lower charge transfer resistance and higher lithium ion diffusion coefficient leading to better electrochemical performance. Therefore, in this study, we synthesized a Sn-doped $LiNi_{0.5}Mn_{1.5-x}Sn_xO_4$ material by a two-step calcination method to obtain materials with high purity, regular particle morphology, and uniform particle size distribution. Moreover, the effects of Sn-doping on the structure and electrochemical properties were further investigated in detail.

EXPERIMENTAL

Material synthesis

In this study all chemical reagents were of A.R. grade. Pure $LiNi_{0.5}Mn_{1.5}O_4$ was prepared by a two-step solid-state method. First, $LiOH{\cdot}H_2O$, $NiCO_3{\cdot}2Ni(OH)_2{\cdot}4H_2O$, and MnO_2 (cationic mole ratio of Li:Ni:Mn = 1.05:0.5:1.5) were mixed in a planetary ball-mill for 3 h using anhydrous ethanol as dispersant. Second, the chemical mixture was dried for 3 h in an air oven followed by grinding of the mixture to fine powder. Then the powder was transferred to a vacuum oven for 6 h. Third, the fine powder was calcined at 800°C for 24 h and then cooled naturally to room temperature, followed by grinding again. Finally the precursor was preheated at 800°C for 0.5 h and calcined at 600°C for 12 h. After naturally cooling to room temperature, the calcined product was ground again to get the pure $LiNi_{0.5}Mn_{1.5}O_4$.

The Sn-doped $LiNi_{0.5}Mn_{1.5}O_4$ composites were obtained through the same method. The raw materials were SnO_2, $LiOH{\cdot}H_2O$, $NiCO_3{\cdot}2Ni(OH)_2{\cdot}4H_2O$, and MnO_2, and the stoichiometric molar ratio of $LiOH{\cdot}H_2O$: $NiCO_3{\cdot}2Ni(OH)_2{\cdot}4H_2O$: MnO_2: SnO_2 was $1.05:0.17:(1.5-x):x$ (x = 0.00, 0.01, 0.02, 0.05, 0.10).

Material characterization

Powder X-ray diffraction (XRD) was performed to characterize the structure of the $LiNi_{0.5}Mn_{1.5-x}Sn_xO_4$ (x = 0, 0.01, 0.02, 0.05, 0.1) with Cu-Kα (40 kV, 30 mA, step size 0.02°, 10°–90°). Structural analyses of the samples were also performed by Raman spectroscopy (Renishaw in Via, Britain) using a 532 nm excitation laser. The particle morphologies of the samples were observed by scanning electron microscopy (SEM, EVOHD 15, Zeiss, German), applying a Quanta-450 SEM instrument to catch the image of the sample. The elemental analyses were performed using an energy dispersive spectrometer (EDS, OCTANE PLUS, EDAX) with operating voltage of 20 kV and minimum spot size of 1 μm.

Electrochemical measurements

The as-prepared materials were mixed with carbon black and polyvinylidene fluoride in a mass ratio of 8:1:1, and then dispersed in *N*-methyl pyrrolidone (NMP) to get a slurry. The slurry was coated onto an aluminum current collector; the cathode material loading was 2–3 mg cm^{-2}. Then the aluminum foil was transferred to an air oven and dried at 80°C, dried in a vacuum oven at 120°C for 4 h, then pressed into circles of diameter 15 mm. CR2025 type coin-cells were assembled in an argon-filled glove box (Universal 2440/750, Mikrouna) with moisture and oxygen content less than 0.1 ppm. High-purity lithium metal was used as the counter electrode, and a polypropylene membrane (Celgard 2400) as the separator. The electrolyte contained 1mol L^{-1} $LiFP_6$ in a 1:1 (v/v) mixture of ethylene carbonate (EC) and dimethyl carbonate (DMC). After assembly, the cells were allowed to rest for 10 h before electrochemical characterization.

Charge-discharge performance was characterized galvanostatically on a Land 2000T (China) tester [30] at various current densities over the voltage range of 3.5–5.0 V *vs.* the Li/Li^+ electrode at ambient temperature (25°C). Cyclic voltammograms (CVs) were recorded with an electrochemical window from 3.5 to 5 V using a CHI 1040B electrochemical workstation with a 0.1 mV s^{-1} scan rate. The electrochemical impedance spectroscopy (EIS) measurement of the cell was performed using a CHI 660a electrochemical workstation with frequency ranging from 0.01 Hz to 100 kHz and alternative current signal amplitude of 5 mV.

RESULTS AND DISCUSSION

The XRD patterns of $LiNi_{0.5}Mn_{1.5-x}Sn_xO_4$ (x = 0, 0.01, 0.02, 0.05 and 0.1) are shown in Fig. 1. According to Fig. 1, the peaks of the samples are similar and all of them match the standard pattern (JCPDS No. 80-2162) apparently, suggesting that a single phase $LiNi_{0.5}Mn_{1.5}O_4$ spinel was obtained. It is worth noting that there are three new peaks at 2θ = 26.5°, 34°, and 52° in the $LiNi_{0.5}Mn_{1.5-x}Sn_xO_4$ (x = 0.02, 0.05, 0.1) samples, which are attributed to SnO_2. Moreover, the intensities of these three peaks in Fig. 1 become stronger with increase in the amount of Sn in the $LiNi_{0.5}Mn_{1.5-x}Sn_xO_4$; it may be caused by the excess of SnO_2 that could not react with other raw materials completely,

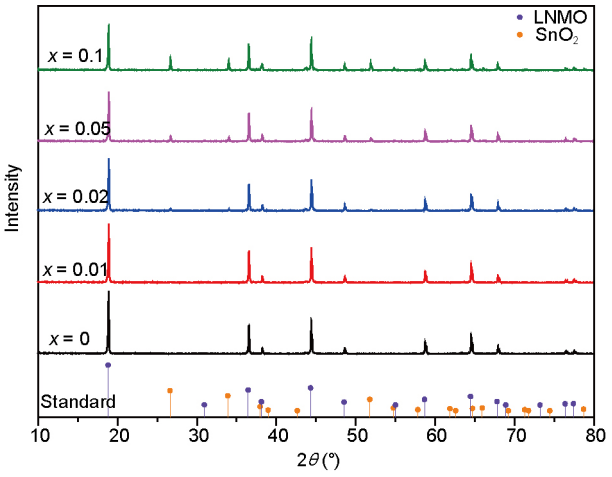

Figure 1 XRD patterns of the two-step-calcination-prepared $LiNi_{0.5}Mn_{1.5-x}Sn_xO_4$ (x = 0, 0.01, 0.02, 0.05, 0.1) and the standard $LiNi_{0.5}Mn_{1.5}O_4$, SnO_2 PDF card.

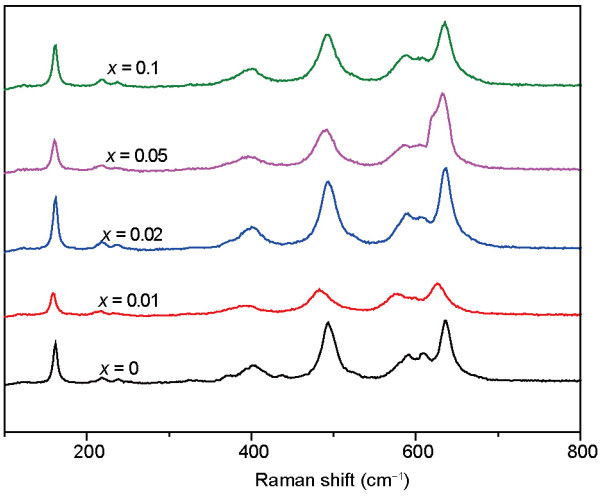

Figure 2 Raman spectra of $LiNi_{0.5}Mn_{1.5-x}Sn_xO_4$ (x = 0, 0.01, 0.02, 0.05, 0.1) powders.

which remained as SnO_2. Therefore, there are specific peaks of SnO_2 in the $LiNi_{0.5}Mn_{1.5-x}Sn_xO_4$ (x = 0.05, 0.1) XRD spectra. Combining the discussions above, the Sn-doped $LiNi_{0.5}Mn_{1.5}O_4$ material has been successfully obtained by this two-step solid-state method.

According to previous reports [31,32], spinel $LiNi_{0.5}Mn_{1.5}O_4$ has two different space groups: the *Fd*-3*m* (F-type) and the $P4_332$ (P-type) space group. To distinguish more clearly the $P4_332$ (P-type) from the *Fd*-3*m* (F-type), Raman spectra were used. The Raman spectra of the $LiNi_{0.5}Mn_{1.5-x}Sn_xO_4$ (x = 0, 0.01, 0.02, 0.05, 0.1) powders are plotted in Fig. 2. Small peaks characteristic of $LiNi_{0.5}Mn_{1.5}O_4$ ordered in the space group $P4_332$ were detected between 200 and 260 cm^{-1} in the samples. According to Oh *et al.* [31,33,34], in the Raman spectrum of $LiNi_{0.5}Mn_{1.5}O_4$ the strong band around 630 cm^{-1} is assigned to the symmetric Mn–O stretching mode of octahedral MnO_6 (A_{1g}), and both peaks around 400 and 490 cm^{-1} are associated with the Ni^{2+}–O stretching mode. The peak near 580–630 cm^{-1} is considered as T_{2g} (3) of the spinel compound. Clear splitting of the T_{2g} (3) band was observed. Thus, the results indicate that all the samples are in the $P4_332$ space group. Meanwhile, with the increase of Sn content, the splitting of T_{2g} (3) band which is related to the symmetric Mn–O stretching mode of MnO_6 octahedral (A_{1g}) gradually lowers. It indicates that the space group changes from $P4_332$ type to *Fd*-3*m* type. Therefore, the introduction of Sn^{4+} contributes to the degree of disorder but does not change the space group. According to Strobel *et al.* [35], the charge difference between Mn and M is the main driving force for such an octahedral cation ordering in $Li_2Mn_3MO_8$. Therefore, in the $LiNi_{0.5}Mn_{1.5-x}Sn_xO_4$ material, the charge difference between Mn and M increases with the increase of Sn^{4+}, resulting in the cation ordering degree decreasing correspondingly.

Fig. 3 shows the SEM micrographs of $LiNi_{0.5}Mn_{1.5-x}Sn_xO_4$ (x = 0, 0.02). As can be seen in Fig. 3a, the $LiNi_{0.5}Mn_{1.5}O_4$ sample has a particle size distribution in the range of 1–2 μm with a little agglomeration, while the $LiNi_{0.5}Mn_{1.48}Sn_{0.02}O_4$ sample has smaller particle size and narrower particle size distribution (Fig. 3c). In the magnified SEM images of the $LiNi_{0.5}Mn_{1.5-x}Sn_xO_4$ (x = 0, 0.02) shown in Fig. 3b, d, the morphologies of $LiNi_{0.5}Mn_{1.5-x}Sn_xO_4$ (x = 0, 0.02) are octahedral, consistent with the result reported by Wang *et al.* [36]. These observations confirm that the addition of Sn^{4+} decreases the particle size slightly but does not significantly change the morphology of $LiNi_{0.5}Mn_{1.5}O_4$. The smaller particle resulted in sufficient contact between the active materials and electrolyte, which is favorable for the diffusion and transmission of Li^+ in the electrode material [37].

In order to prove that Sn^{4+} was homogeneously doped in $LiNi_{0.5}Mn_{1.5}O_4$, EDS mapping images and EDS spectrum of x = 0.02 material are shown in Fig. 4. According to Fig. 4b–f, the presence of Sn, Mn, Ni, and O can be found. In the EDS spectrum of $LiNi_{0.5}Mn_{1.5-x}Sn_xO_4$ (x = 0.02) (Fig. 4g), most of the elements found on the surface are Mn, Ni, Sn, and O from the $LiNi_{0.5}Mn_{1.5-x}Sn_xO_4$ particles. These images confirm that Sn^{4+} has been doped in the $LiNi_{0.5}Mn_{1.5}O_4$ material successfully and that the distribution of Sn is homogeneous.

Fig. 5 shows the charge-discharge curves of the prepared

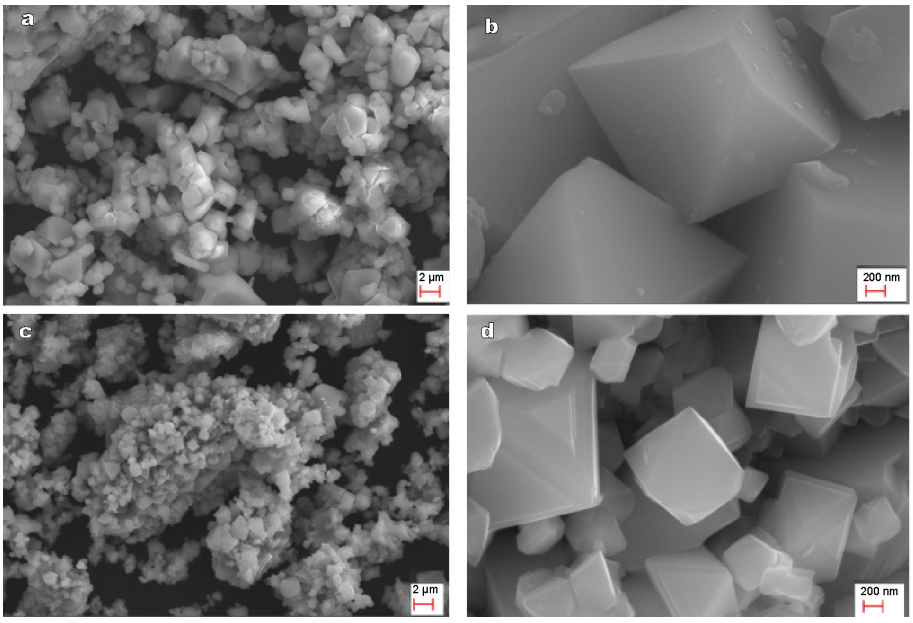

Figure 3 SEM images of $LiNi_{0.5}Mn_{1.5-x}Sn_xO_4$: (a, b) $x = 0$ and (c, d) $x = 0.02$, respectively.

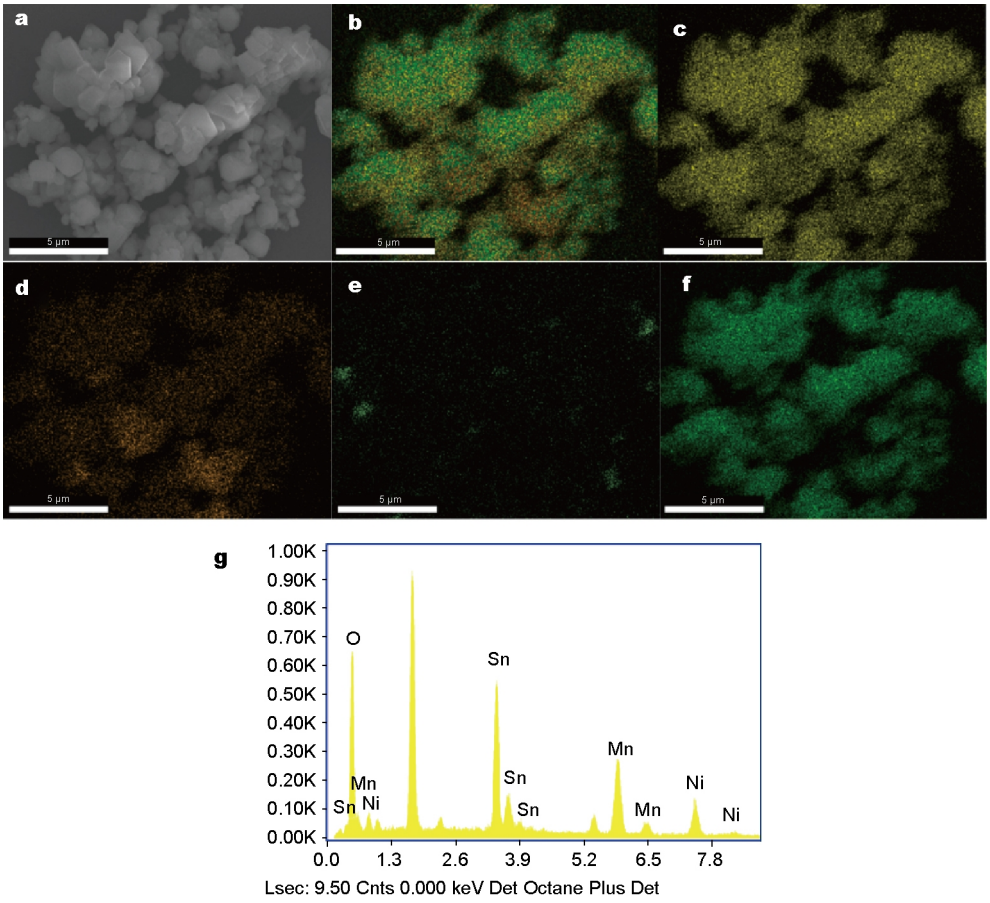

Figure 4 EDS mapping images and EDS profile of the $LiNi_{0.5}Mn_{1.48}Sn_{0.02}O_4$ composite. (a) SEM image of $LiNi_{0.5}Mn_{1.48}Sn_{0.02}O_4$, (b) EDS maps of $LiNi_{0.5}Mn_{1.48}Sn_{0.02}O_4$, (c) Mn element (d) Ni element, (e) Sn element, (f) O element, (g) EDS profile.

$LiNi_{0.5}Mn_{1.5-x}Sn_xO_4$ (x = 0, 0.01, 0.02, 0.05, 0.1) materials carried out at room temperature in the 3.5–4.9 V range, at a current density of 0.1 C. There is an obvious plateau around 4.7 V, which reflects the Ni^{2+}/Ni^{4+} redox reaction [38], and the cells of x = 0, 0.01, 0.02, 0.05, 0.1 exhibit discharge capacities about 101, 109.5, 117.9, 94, 85.6 mA h g^{-1} at 0.1 C, respectively. In comparison, $LiNi_{0.5}Mn_{1.5-x}Sn_xO_4$ (x = 0.02) exhibits the highest discharge capacity and delivers a discharge capacity ~16% higher than the undoped $LiNi_{0.5}Mn_{1.5}O_4$.

According to other studies [4,39,40], the plateau around 4.0 V reflects the redox reaction of the Mn^{3+}/Mn^{4+} couple. However, the 4.0 V plateaus of our materials are too tiny to be distinguished, indicating that a small amount of Mn^{3+} exists in the samples [34]. This result is consistent with the Raman results mentioned above, indicating that the space group of the material synthesized by two-step calcination was $P4_332$ (P-type).

The cyclic performances of $LiNi_{0.5}Mn_{1.5-x}Sn_xO_4$ (x = 0, 0.01, 0.02, 0.05, 0.1) at 1 C in the potential range of 3.5–4.9 V at room temperature are shown in Fig. 6. It can be observed from Fig. 6 that all the Sn-doping materials give higher specific discharge capacity at the rate of 1 C after 100 cycles than the undoped material. The discharge capacity of the undoped $LiNi_{0.5}Mn_{1.5}O_4$ was 56.1 mA h g^{-1} after 100 cycles, and the discharge capacity retention was only 93.34%. However, the discharge capacities of the $LiNi_{0.5}Mn_{1.5-x}Sn_xO_4$ (x = 0.01, 0.02, 0.05, and 0.1) samples were improved to various degrees. When x = 0.01, the discharge capacities of the 1st and 100th cycles were 74.9 and 70.6 mA h g^{-1}, respectively, at 1 C, with discharge retention of 94.25%. When x = 0.02, the discharge capacities of the 1st and 100th cycles were 92 and 90 mA h g^{-1}, respectively, with discharge retention of 97.84%. When x = 0.05 and x = 0.1, the discharge capacities of the 100th cycles were 65.1 and 61 mA h g^{-1}, respectively. In comparison, the $LiNi_{0.5}Mn_{1.5-x}Sn_xO_4$ (x = 0.02) material has higher specific capacity retention and cycle performance than $LiNi_{0.5}Mn_{1.5-x}Sn_xO_4$ (x = 0, 0.01, 0.05, 0.1), with initial specific capacity of 92 mA h g^{-1} and smaller specific capacity fade. The excellent cycle performance could be attributed to the structural stability. A small amount of Sn^{4+} doping could stabilize the structure of the material, whereas the existence of too many Sn^{4+} cations in the crystal lattice may induce large changes to the structure and cause irreversible phase transfer [17,41]. The capacity increases slightly at the outset, which is attributed to the expansion of the electrode materials and the electrolyte wetting the electrode material during the charge-discharge progress [35].

Fig. 7 shows the typical steady-state CVs of $LiNi_{0.5}Mn_{1.5-x}Sn_xO_4$ (x = 0, 0.01, 0.02, 0.05, 0.1). The CV profiles were recorded in the range of 3.5–5 V *vs.* Li^+/Li at a scan rate of 0.1 mV s^{-1}. Compared with other studies [38,41–44], there are no peaks around 4.0 V that may be caused by Mn^{3+}, corresponding to the first charge-discharge curve. Compared with other reports [34,45], the anodic peak and cathodic peak around 4.7 V (*vs.* Li^+/Li) broadens obviously, which corresponds to the redox reaction of Ni^{2+}/Ni^{4+}. Meanwhile, the voltage difference between the anodic and cathodic peaks reflects the degree of polarization of the electrode, and is also affected by the degree of disorder of the cations and the extraction/rein-sertion rate of Li^+ in the spinel structure [45,46]. To understand the reversibility of the electrode material, we calculated the voltage differences between the two split peaks near 4.7 V. Results are shown in Table 1. ΔEp for

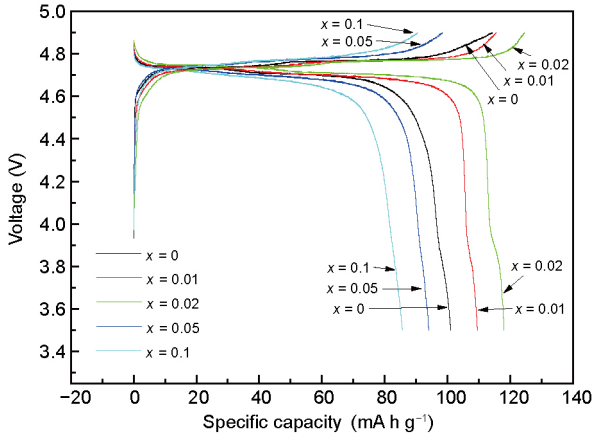

Figure 5 Charge-discharge curves of the $LiNi_{0.5}Mn_{1.5-x}Sn_xO_4$ (x = 0, 0.01, 0.02, 0.05, 0.1) at 0.1 C.

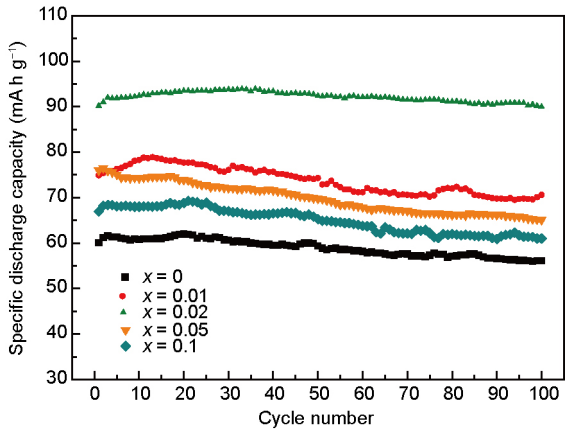

Figure 6 Cycle life performances of $LiNi_{0.5}Mn_{1.5-x}Sn_xO_4$ (x = 0, 0.01, 0.02, 0.05, 0.1) at 1 C.

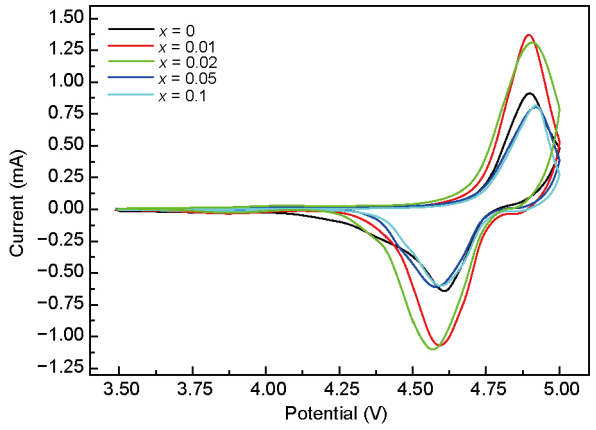

Figure 7 CV plots of the $LiNi_{0.5}Mn_{1.5-x}Sn_xO_4$ (x = 0, 0.01, 0.02, 0.05, 0.1) cells in the range of 3.5–5 V at the scanning rate of 0.1 mV s^{-1}.

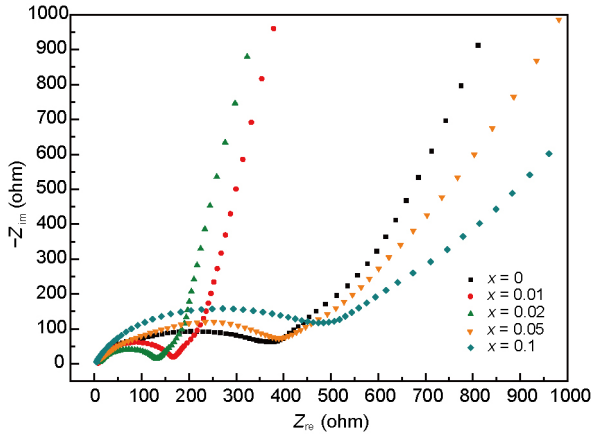

Figure 8 Nyquist plots of the $LiNi_{0.5}Mn_{1.5-x}Sn_xO_4$ (x = 0, 0.01, 0.02, 0.05, 0.1) cells, after charging to 4.8 V (*vs.* Li), respectively.

x = 0 is less than any of the other cells. With increasing Sn^{4+}, the degree of disorder of the cations increases correspondingly, resulting in larger polarization and irreversibility. The value of ΔEp for $LiNi_{0.5}Mn_{1.5-x}Sn_xO_4$ (x = 0.02, 0.05, 0.1) are similiar. It can be concluded that an excess amount of Sn-doping has negligible impact on the reversibility of the electrode.

To comprehensively understand the improvement of the electrochemical performance after Sn-doping, EIS measurements were carried out. The electrochemical dynamic behaviors of the $LiNi_{0.5}Mn_{1.5-x}Sn_xO_4$ (x = 0, 0.01, 0.02, 0.05, 0.1) cells were analyzed and the results are shown in Fig. 8. In the plot there are five semicircles in the high frequency range, which corresponds to the charge-transfer resistance. Meanwhile, there are five straight lines with different slopes at low frequency, which are related to the lithium-diffusion process [47]. It is convincing that the resistance of $LiNi_{0.5}Mn_{1.5-x}Sn_xO_4$ (x = 0.02) is obviously lower than the other samples, indicating a higher lithium-diffusion coefficient and lower charge-transfer resistance of the $LiNi_{0.5}Mn_{1.5-x}Sn_xO_4$ (x = 0.02) material than the primitive $LiNi_{0.5}Mn_{1.5}O_4$ material.

Further, we calculated the values of R_s and R_{ct}, which are related to the resistance of the electrolyte and the charge transfer resistance at the particle/electrolyte interface, respectively [47]. The results are shown in Table 2. Comparing the results for R_s, there is little influence on R_s after Sn-doping, while R_{ct} changes markedly. With the increase of the amount of Sn-doping, the R_{ct} reduces, whereas when the amount of Sn-doping rises to 0.05, R_{ct} increases dramatically. It may be caused by excess Sn^{4+} blocking the transfer path of electrons and increasing the resistance.

Furthermore, we calculated the lithium ion diffusion coefficient from the EIS plots in the low-frequency region according to the following equations [48]:

$$D_{Li} = 0.5\left(RT/An^2F^2\sigma_\omega C_{Li}\right)^2, \quad (1)$$

$$Z_{re} = R_s + R_{ct} + \sigma_\omega \omega^{-0.5}, \quad (2)$$

where R is the gas constant, T is the absolute temperature, ω is the angular frequency, n represents the number of electrons per molecule during oxidization, F is Faraday's constant, C_{Li} is the concentration of lithium ion in the solid, and σ is the Warburg factor. The Z_{re}-$\omega^{-0.5}$ plots of the cells mentioned above are presented in Fig. 9. The values of ω for $LiNi_{0.5}Mn_{1.5-x}Sn_xO_4$ (x = 0, 0.01, 0.02, 0.05, 0.1) are

Table 1 Redox peaks of the $LiNi_{0.5}Mn_{1.5-x}Sn_xO_4$ (x = 0, 0.01, 0.02, 0.05, 0.1) material

$LiNi_{0.5}Mn_{1.5-x}Sn_xO_4$	Ep_a (V)	Ep_c (V)	ΔEp (mV)
x = 0	4.900	4.609	291
x = 0.01	4.895	4.593	302
x = 0.02	4.907	4.567	340
x = 0.05	4.919	4.579	340
x = 0.1	4.92	4.595	325

Table 2 R_s and R_{ct} values of $LiNi_{0.5}Mn_{1.5-x}Sn_xO_4$ (x = 0, 0.01, 0.02, 0.05, 0.1)

x	R_s (ohm)	R_{ct} (ohm)
0	10.68	380.8
0.01	7.768	155.5
0.02	7.998	127.6
0.05	7.467	407.2
0.1	4.67	460.5

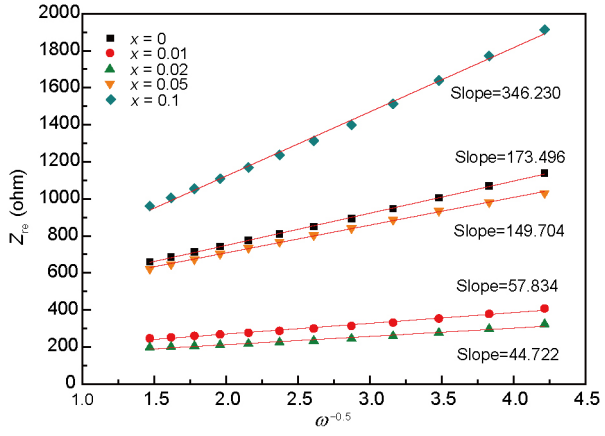

Figure 9 Relationship between Z_{re} and $\omega^{-0.5}$ of $LiNi_{0.5}Mn_{1.5-x}Sn_xO_4$ (x = 0, 0.01, 0.02, 0.05, 0.1) in the low-frequency region.

173.469, 57.834, 44.722, 149.704, and 346.230, respectively. The diffusion coefficient of lithium ion is calculated based on Equations (1) and (2) and the results show that the $LiNi_{0.5}Mn_{1.5-x}Sn_xO_4$ (x = 0.02) has a diffusion coefficient of 3.916×10^{-15} cm^2 s^{-1}, higher than that of the other materials which are 1.033×10^{-15}, 2.366×10^{-15}, 0.3406×10^{-15} and 0.0639×10^{-15} cm^2 s^{-1} for x = 0, 0.01, 0.05, 0.1, respectively. This result indicates that the mobility of lithium ions in $LiNi_{0.5}Mn_{1.5}O_4$ can be effectively improved by Sn doping.

CONCLUSIONS

$LiNi_{0.5}Mn_{1.5-x}Sn_xO_4$ (x = 0, 0.01, 0.02, 0.05, 0.1) materials were synthesized by a solid-state two-step calcination method. Sn doping contributes to the degree of disorder, leading to better electrochemical performance. However, Sn-doping does not change the space group; all the materials maintained the spinel structure with $P4_332$ space group. Based on the discussion mentioned above, we can conclude that the $LiNi_{0.5}Mn_{1.48}Sn_{0.02}O_4$ material shows the superior specific capacity of 117.9 mA h g^{-1} at the first cycle, and has a better rate capability than the primitive $LiNi_{0.5}Mn_{1.5}O_4$ material. Meanwhile, the $LiNi_{0.5}Mn_{1.48}Sn_{0.02}O_4$ material retains 97.84% capacity retention after 100 cycles at charge-discharge rate 1 C and the rate performance of $LiNi_{0.5}Mn_{1.5}O_4$ is also greatly improved by Sn-doping. Moreover, the significantly enhanced D_{Li^+} and the enlarged electronic conductivity make the Sn-doped spinel $LiNi_{0.5}Mn_{1.5}O_4$ material present even better electrochemical performances, suggesting that the idea of Sn-doping has a positive effect.

Received 2 December 2016; accepted 7 January 2017; published online 22 January 2017

1 Liu H, Wang J, Zhang X, *et al.* Morphological evolution of high-voltage spinel $LiNi_{0.5}Mn_{1.5}O_4$ cathode materials for lithium-ion batteries: the critical effects of surface orientations and particle size. ACS Appl Mater Interfaces, 2016, 8: 4661–4675
2 Jin YC, Duh JG. Nanostructured $LiNi_{0.5}Mn_{1.5}O_4$ cathode material synthesized by polymer-assisted co-precipitation method with improved rate capability. Mater Lett, 2013, 93: 77–80
3 Wang L, Chen D, Wang J, *et al.* Synthesis of $LiNi_{0.5}Mn_{1.5}O_4$ cathode material with improved electrochemical performances through a modified solid-state method. Powder Tech, 2016, 292: 203–209
4 Yi TF, Mei J, Zhu YR. Key strategies for enhancing the cycling stability and rate capacity of $LiNi_{0.5}Mn_{1.5}O_4$ as high-voltage cathode materials for high power lithium-ion batteries. J Power Sources, 2016, 316: 85–105
5 Fang X, Shen C, Ge M, *et al.* High-power lithium ion batteries based on flexible and light-weight cathode of $LiNi_{0.5}Mn_{1.5}O_4$/carbon nanotube film. Nano Energy, 2015, 12: 43–51
6 Liu D, Trottier J, Charest P, *et al.* Effect of nano $LiFePO_4$ coating on $LiMn_{1.5}Ni_{0.5}O_4$ 5 V cathode for lithium ion batteries. J Power Sources, 2012, 204: 127–132
7 Hwang T, Lee JK, Mun J, *et al.* Surface-modified carbon nanotube coating on high-voltage $LiNi_{0.5}Mn_{1.5}O_4$ cathodes for lithium ion batteries. J Power Sources, 2016, 322: 40–48
8 Yi TF, Chen B, Zhu YR, *et al.* Enhanced rate performance of molybdenum-doped spinel $LiNi_{0.5}Mn_{1.5}O_4$ cathode materials for lithium ion battery. J Power Sources, 2014, 247: 778–785
9 Wang S, Li P, Shao L, *et al.* Preparation of spinel $LiNi_{0.5}Mn_{1.5}O_4$ and Cr-doped $LiNi_{0.5}Mn_{1.5}O_4$ cathode materials by tartaric acid assisted sol–gel method. Ceramics Int, 2015, 41: 1347–1353
10 Hu CL, Yi HH, Wang FX, *et al.* Boron doping at P-site to improve electrochemical performance of $LiMnPO_4$ as cathode for lithium ion battery. J Power Sources, 2014, 255: 355–359
11 Alcántara R, Jaraba M, Lavela P, *et al.* Structural and electrochemical study of new $LiNi_{0.5}Ti_xMn_{1.5-x}O_4$ spinel oxides for 5-V cathode materials. Chem Mater, 2003, 15: 2376–2382
12 Zhong GB, Wang YY, Zhang ZC, *et al.* Effects of Al substitution for Ni and Mn on the electrochemical properties of $LiNi_{0.5}Mn_{1.5}O_4$. Electrochim Acta, 2011, 56: 6554–6561
13 Prabakar SJR, Han SC, Singh SP, *et al.* W-doped $LiW_xNi_{0.5}Mn_{1.5-x}O_4$ cathodes for the improvement of high rate performances in Li ion batteries. J Power Sources, 2012, 209: 57–64
14 Liu H, Bi S, Wen G, *et al.* Synthesis and electrochemical performance of Sn-doped $Li_3V_2(PO_4)_3$/C cathode material for lithium ion battery by microwave solid-state technique. J Alloy Compd, 2012, 543: 99–104
15 Ma X, Wang C, Cheng J, *et al.* Effects of Sn doping on the structural and electrochemical properties of $LiNi_{0.8}Co_{0.2}O_2$ cathode materials. Solid State Ionics, 2007, 178: 125–129
16 Zhang B, Huang ZD, Oh SW, *et al.* Improved rate capability of carbon coated $Li_{3.9}Sn_{0.1}Ti_5O_{12}$ porous electrodes for Li-ion batteries. J Power Sources, 2011, 196: 10692–10697
17 Ma J, Li B, Du H, *et al.* Effects of tin doping on physicochemical and electrochemical performances of $LiFe_{1-x}Sn_xPO_4$/C ($0\le x\le0.07$) composite cathode materials. Electrochim Acta, 2011, 56: 7385–7391
18 Yoon J, Kim D, Um JH, *et al.* Effect of local structural changes on rate capability of $LiNi_{0.5}Mn_{1.5}O_{4-\delta}$ cathode material for lithium ion batteries. J Alloy Compd, 2016, 686: 593–600
19 Jia G, Jiao C, Xue W, *et al.* Improvement in electrochemical performance of calcined $LiNi_{0.5}Mn_{1.5}O_4$/GO. Solid State Ionics, 2016, 292: 15–21

20 Jiao C, Wang L, Zuo Y, *et al.* Solid-state synthesis of spherical hierarchical $LiNi_{0.5}Mn_{1.5}O_4$ through an improved calcination method and its cyclic performance for 5 V lithium ion batteries. Solid State Ionics, 2015, 277: 50–56
21 Liu H, Wu YP, Rahm E, *et al.* Cathode materials for lithium ion batteries prepared by sol-gel methods. J Solid State Electrochem, 2004, 8: 450–466
22 Lee YS, Sun YK, Ota S, *et al.* Preparation and characterization of nano-crystalline $LiNi_{0.5}Mn_{1.5}O_4$ for 5 V cathode material by composite carbonate process. Electrochem Commun, 2002, 4: 989–994
23 Fan Y, Wang J, Ye X, *et al.* Physical properties and electrochemical performance of $LiNi_{0.5}Mn_{1.5}O_4$ cathode material prepared by a co-precipitation method. Mater Chem Phys, 2007, 103: 19–23
24 Li D, Ito A, Kobayakawa K, *et al.* Electrochemical characteristics of $LiNi_{0.5}Mn_{1.5}O_4$ prepared by spray drying and post-annealing. Electrochim Acta, 2007, 52: 1919–1924
25 Caballero A, Hernán L, Melero M, *et al.* $LiNi_{0.5}Mn_{1.5}O_4$ thick-film electrodes prepared by electrophoretic deposition for use in high voltage lithium-ion batteries. J Power Sources, 2006, 158: 583–590
26 Xia H, Tang SB, Lu L, *et al.* The influence of preparation conditions on electrochemical properties of $LiNi_{0.5}Mn_{1.5}O_4$ thin film electrodes by PLD. Electrochim Acta, 2007, 52: 2822–2828
27 Kim JH, Myung ST, Sun YK. Molten salt synthesis of $LiNi_{0.5}Mn_{1.5}O_4$ spinel for 5 V class cathode material of Li-ion secondary battery. Electrochim Acta, 2004, 49: 219–227
28 Myung ST, Komaba S, Kumagai N, *et al.* Nano-crystalline $LiNi_{0.5}Mn_{1.5}O_4$ synthesized by emulsion drying method. Electrochim Acta, 2002, 47: 2543–2549
29 Liu Y, Zhang M, Xia Y, *et al.* One-step hydrothermal method synthesis of core–shell $LiNi_{0.5}Mn_{1.5}O_4$ spinel cathodes for Li-ion batteries. J Power Sources, 2014, 256: 66–71
30 Liu H, Wen G, Bi S, *et al.* Enhanced rate performance of nanosized $Li_4Ti_5O_{12}$/graphene composites as anode material by a solid state-assembly method. Electrochim Acta, 2015, 171: 114–120
31 Oh SH, Chung KY, Jeon SH, *et al.* Structural and electrochemical investigations on the $LiNi_{0.5-x}Mn_{1.5-y}M_{x+y}O_4$ (M=Cr, Al, Zr) compound for 5V cathode material. J Alloy Compd, 2009, 469: 244–250
32 Kim JH, Myung ST, Yoon CS, *et al.* Comparative study of $LiNi_{0.5}Mn_{1.5}O_{4-\delta}$ and $LiNi_{0.5}Mn_{1.5}O_4$ cathodes having two crystallographic structures: $Fd\bar{3}m$ and $P4_332$. Chem Mater, 2004, 16: 906–914
33 Julien CM, Massot M. Lattice vibrations of materials for lithium rechargeable batteries I. Lithium manganese oxide spinel. Mater Sci Eng-B, 2003, 97: 217–230
34 Wang L, Li H, Huang X, *et al.* A comparative study of *Fd*-3*m* and *P*4332 "$LiNi_{0.5}Mn_{1.5}O_4$". Solid State Ionics, 2011, 193: 32–38
35 Strobel P, Ibarra-Palos A, Anne M, *et al.* Cation ordering in $Li_2Mn_3MO_8$ spinels: structural and vibration spectroscopy studies. Solid State Sci, 2003, 5: 1009–1018
36 Wang H, Xia H, Lai MO, *et al.* Enhancements of rate capability and cyclic performance of spinel $LiNi_{0.5}Mn_{1.5}O_4$ by trace Ru-doping. Electrochem Commun, 2009, 11: 1539–1542
37 Kovacheva D, Markovsky B, Salitra G, *et al.* Electrochemical behavior of electrodes comprising micro- and nano-sized particles of $LiNi_{0.5}Mn_{1.5}O_4$: a comparative study. Electrochim Acta, 2005, 50: 5553–5560
38 Yi TF, Fang ZK, Xie Y, *et al.* Synthesis of $LiNi_{0.5}Mn_{1.5}O_4$ cathode with excellent fast charge-discharge performance for lithium-ion battery. Electrochim Acta, 2014, 147: 250–256
39 Feng J, Huang Z, Guo C, *et al.* An organic coprecipitation route to synthesize high voltage $LiNi_{0.5}Mn_{1.5}O_4$. ACS Appl Mater Interfaces, 2013, 5: 10227–10232
40 Monaco S, De Giorgio F, Da Col L, *et al.* Electrochemical performance of $LiNi_{0.5}Mn_{1.5}O_4$ composite electrodes featuring carbons and reduced graphene oxide. J Power Sources, 2015, 278: 733–740
41 Ai D, Liu K, Lu Z, *et al.* Aluminothermal synthesis and characterization of $Li_3V_{2-x}Al_x(PO_4)_3$ cathode materials for lithium ion batteries. Electrochim Acta, 2011, 56: 2823–2827
42 Liu J, Liu W, Ji S, *et al.* Electrospun spinel $LiNi_{0.5}Mn_{1.5}O_4$ hierarchical nanofibers as 5 V cathode materials for lithium-ion batteries. ChemPlusChem, 2013, 78: 636–641
43 Xiao L, Zhao Y, Yang Y, *et al.* Electrochemical properties of nano-crystalline $LiNi_{0.5}Mn_{1.5}O_4$ synthesized by polymer-pyrolysis method. J Solid State Electrochem, 2008, 12: 687–691
44 Yang T, Zhang N, Lang Y, *et al.* Enhanced rate performance of carbon-coated $LiNi_{0.5}Mn_{1.5}O_4$ cathode material for lithium ion batteries. Electrochim Acta, 2011, 56: 4058–4064
45 Liu J, Manthiram A. Understanding the improved electrochemical performances of Fe-substituted 5 V spinel cathode $LiMn_{1.5}Ni_{0.5}O_4$. J Phys Chem C, 2009, 113: 15073–15079
46 Zhong GB, Wang YY, Zhao XJ, *et al.* Structural, electrochemical and thermal stability investigations on $LiNi_{0.5-x}Al_{2x}Mn_{1.5-x}O_4$ ($0 \le 2x \le 1.0$) as 5 V cathode materials. J Power Sources, 2012, 216: 368–375
47 Liu H, Wen G, Bi S, *et al.* High rate cycling performance of nanosized $Li_4Ti_5O_{12}$/graphene composites for lithium ion batteries. Electrochim Acta, 2016, 192: 38–44
48 Cao Q, Zhang HP, Wang GJ, *et al.* A novel carbon-coated $LiCoO_2$ as cathode material for lithium ion battery. Electrochem Commun, 2007, 9: 1228–1232

Acknowledgments This work was supported by the Science and Technology Program of WeiHai (2015DXGJMS017), and HIT & Yun Shan Group Research and Development on Graphite Area.

Author contributions Liu H convinced the idea of the research; Hao J performed the experiments and wrote the manuscript. All authors contributed to the general discussion.

Conflict of interest The authors declare that they have no conflict of interest.

Jingmin Hao is currently a graduate student majored in electrochemistry at the School of Marine Science and Technology, Harbin Institute of Technology, Weihai. Her research interest includes tuning the morphology of $LiNi_{0.5}Mn_{1.5}O_4$ to optimize its electrochemical properties.

Haiping Liu received her BSc degree in chemical engineering from Qilu University of Technology in 1998, and her MSc and PhD degrees in chemical engineering and technology in 2004 and 2008, respectively, from Harbin Institute of Technology. Then, she joined Harbin Institute of Technology, Weihai as a faculty and became an associate professor of applied chemistry in 2013. Her research interests include electrodeposition, surface finishing, electrode materials, and graphene composite materials for Li-ion batteries.

锡掺杂$LiNi_{0.5}Mn_{1.5}O_4$锂离子电池高电压正极材料的制备及性能研究

郝晶敏[1], 刘海萍[1*], 吉元鹏[1], 毕四富[2]

摘要 本文采用两步烧结高温固相法成功制备了锡掺杂$LiNi_{0.5}Mn_{1.5-x}Sn_xO_4$ ($0 \leqslant x \leqslant 0.1$)锂离子电池正极材料. x为0.02时, $LiNi_{0.5}Mn_{1.48}Sn_{0.02}O_4$的比容量和循环性能最好. 室温下, 在3.5–4.9 V电压范围内, 0.1 C放电倍率, $LiNi_{0.5}Mn_{1.48}Sn_{0.02}O_4$的首次放电比容量为117 mA h g^{-1}, 而没有锡掺杂的$LiNi_{0.5}Mn_{1.5}O_4$只有101 mA h g^{-1}. 此外, 1 C放电100个循环后, 所有锡掺杂后的$LiNi_{0.5}Mn_{1.5}O_4$材料均保持了较高的放电比容量; 尤其是$LiNi_{0.5}Mn_{1.48}Sn_{0.02}O_4$, 100个循环后, 放电比容量为90 mA h g^{-1}, 而纯的$LiNi_{0.5}Mn_{1.5}O_4$, 100个循环后其放电比容量仅为56.1 mA h g^{-1}. 锡掺杂后的$LiNi_{0.5}Mn_{1.48}Sn_{0.02}O_4$材料具有比$LiNi_{0.5}Mn_{1.5}O_4$材料及其他组材料更高的锂离子扩散效率, Sn离子的掺杂有利于锂离子的扩散和导电性的提高, 从而提高了$LiNi_{0.5}Mn_{1.5}O_4$的电化学性能. 因此锡掺杂是一种有效的改善高电压锂离子电池材料$LiNi_{0.5}Mn_{1.5}O_4$电化学性能的方法.